# Single-domain model for toggle MRAM

An overview is presented of the use of a single-domain model for developing an understanding of the switching of two coupled magnetic free layers for toggle MRAM (magnetic random access memory). The model includes the effects of length, width, thickness, magnetization, thickness asymmetry, intrinsic anisotropy, exchange coupling, dipole coupling, and applied magnetic field. First, a simple perturbative approach is used to understand the basic phenomena at low fields, including the critical switching curve and activation energy. Then the more general model is applied in order to understand the effects of saturation at large field, and thickness asymmetry. The major results are that toggle MRAM should have a larger margin for half-select and full-select switching fields than Stoner—Wohlfarth MRAM, and that the activation energy should increase upon half-select, thus eliminating the half-select activated-error problem.

## Introduction: Why is toggle MRAM better than Stoner–Wohlfarth MRAM?

In traditional MRAM, use is made of a single free layer [see Figure 1(a)] which switches by Stoner-Wohlfarth reversal [1]. As shown in Figure 1(b), for fields applied outside the astroid boundary only one state is stable, whereas at T = 0, for fields inside the astroid boundary both states are stable and no switching occurs between them. Switching is accomplished by simultaneously applying both bit-line and word-line fields (full-select) to the selected bit. Since this full-select field is outside the astroid boundary, the selected bit is stable only in the state to be written. At the same time, the other "halfselected" bits on the same bit line and word line do not switch because the half-select field is inside the astroid boundary. This Stoner–Wohlfarth method of switching has two major disadvantages. The first is that the margin between half select and full select is small; this would require tight control of the switching fields in order to reach the multi-megabit chip level. The second disadvantage is that for  $T \neq 0$ , there is a large drop in the activation energy for half-selected bits, as shown in Figure 1(c). This activation energy is the barrier preventing the bit from making a thermally activated switch into the other state. The drop in the activation energy, combined with the large number of half selects which occur over the lifetime of the chip, results in a

significant error rate. These two problems, half-select margin and activated errors, limit the usefulness of Stoner–Wohlfarth MRAM to small arrays and short lifetimes.

Leonid Savtchenko invented a solution to these problems, known as toggle MRAM [2]. As shown in Figure 1(d), in spin-flop switching the single free layer is replaced by two magnetic layers separated by a nonmagnetic spacer layer. This dramatically changes the shape of the critical switching curve, as shown in Figure 1(e) [2]. The bit can now tolerate a half-select field many times larger than the smallest required full-select field, thus relaxing the requirement on control of the switching fields from bit to bit. Furthermore, as shown in Figure 1(f), the activation energy under half-select actually increases, thus making the bit more rather than less thermally stable [3]. This essentially eliminates the activated-error problem.

Figures 1 and 2 capture the essence of the difference between the Stoner–Wohlfarth and toggle MRAM approaches. The rest of this paper explains these approaches in more detail. The next section gives an overview of toggling and spin-flop switching. Then a simple perturbative model is introduced which gives an intuitive but approximate description of the switching behavior at small fields for the special case of a circular balanced bit. Finally, an exact single-domain model is

©Copyright 2006 by International Business Machines Corporation. Copying in printed form for private use is permitted without payment of royalty provided that (1) each reproduction is done without alteration and (2) the Journal reference and IBM copyright notice are included on the first page. The title and abstract, but no other portions, of this paper may be copied or distributed royalty free without further permission by computer-based and other information-service systems. Permission to republish any other portion of this paper must be obtained from the Editor.

0018-8646/06/\$5.00 © 2006 IBM



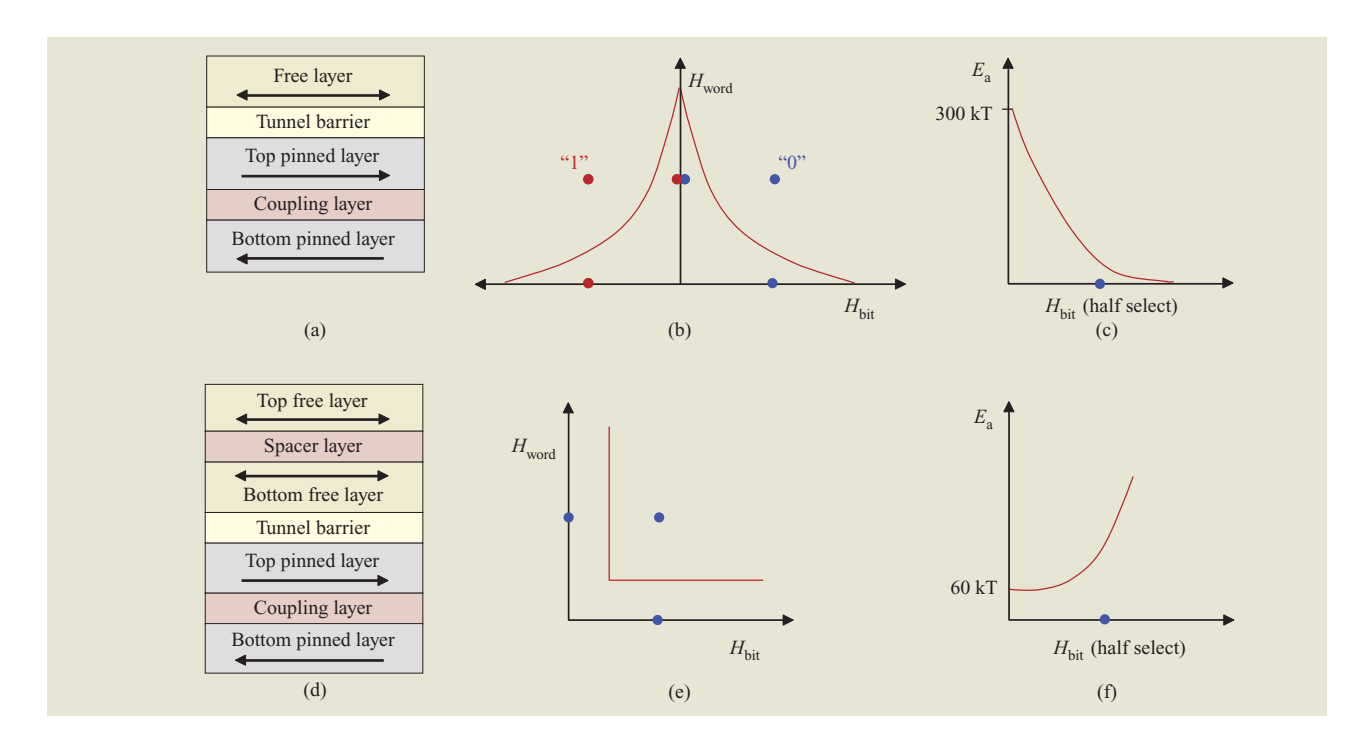


Figure 1

Illustrative switching by Stoner–Wohlfarth reversal and toggle MRAM. In traditional Stoner–Wohlfarth switching, use is made of a single free layer, as shown in the tunnel junction cross section (a), which switches when a field is applied across the critical switching curve, or "astroid" (b). When a field is applied along the half-select direction, the activation energy decreases dramatically (c). In toggle switching, use is made of two magnetic free layers (d), which switch when a rectangular field excursion crosses the L-shaped critical switching curve (e). When a field is applied along the half-select direction, the activation energy initially increases, making the bit more stable (f).

described and used to explain the switching behavior in general.

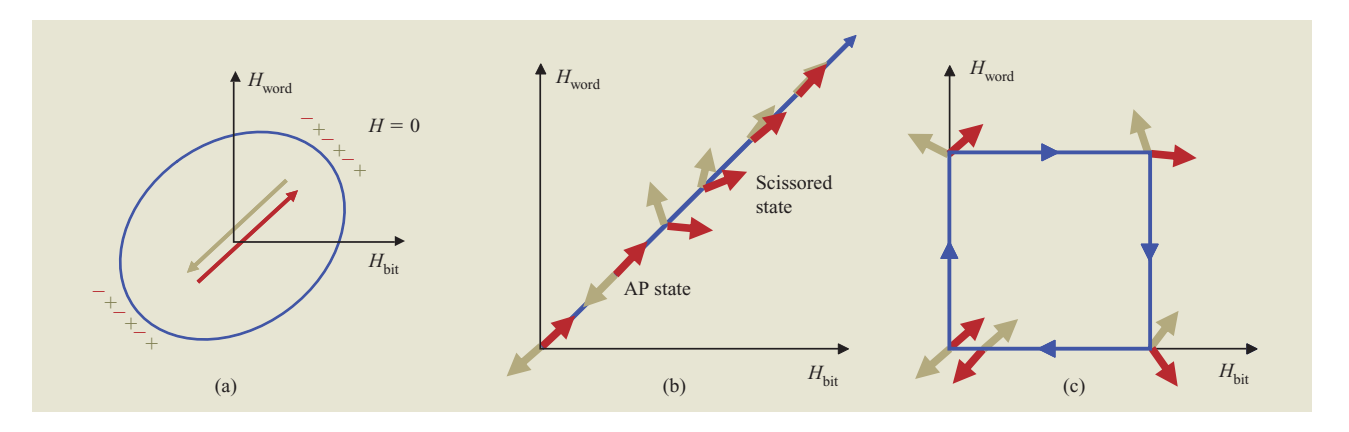
Portions of this work have previously been published in more abbreviated form in [3] and [4]. A similar single-domain model has been discussed in [5]. Experimental results on toggle MRAM have been reported in [2, 6, 7].

#### Overview of toggling and spin-flop switching

As shown in Figure 1(d), the toggle bit has two magnetic layers of equal thickness t, which are separated by a nonmagnetic spacer. Figure 2(a) shows a top-down view of the bit, which is patterned in the shape of an ellipse or circle. The magnetic poles formed at the edges of each of the two magnetic layers create dipole fields, which make the two layers line up anti-parallel (AP) in zero field. (It is also possible to add some exchange coupling from the spacer layer, though this is optional.) This flux closure has several ramifications. First, in this flux-closed anti-parallel state, the shape anisotropy does not determine the orientation of the moments in zero field, since there is no net moment. Instead, the zero-field orientation is determined by the intrinsic anisotropy of the two magnetic layers, which is chosen to lie at 45 degrees to the

bit lines and word lines (by depositing and annealing the films in a magnetic field). This direction is termed the easy axis. Second, the zero-field activation energy is set by the intrinsic anisotropy, not by the shape anisotropy, as in Stoner–Wohlfarth switching. Finally, the flux closure results in an appreciable reduction in the bit-to-bit dipole field coupling.

When a magnetic field is applied along the easy axis of the bit [Figure 2(b)], the moments initially do not respond. This is because there is no net moment for the field to act upon. As the easy-axis field is increased, the AP state is maintained until a critical field, known as the spin-flop field  $H_{\rm sf}$ , is reached; at this point the moments discontinuously jump from the AP state into a "scissored" state. In the scissored state the net moment is pointing in the direction of the applied field, with one moment rotated clockwise and the other moment rotated counterclockwise from this direction. In that state there is a net moment, and as the field is further increased, the moments respond by smoothly scissoring together until they become parallel at a field  $H_{xsat}$ . This spin-flop phenomenon is familiar from the study of antiferromagnets, but is usually accessible only



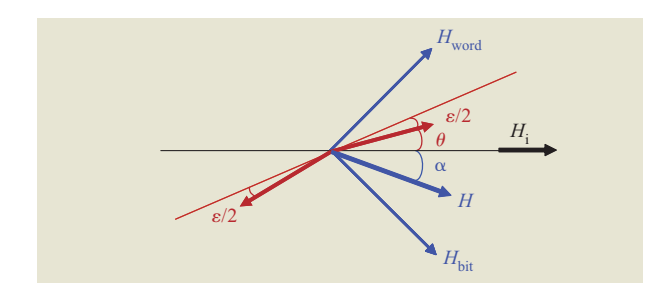
(a) Top view of a toggle bit in an MRAM. In zero field, the moments line up anti-parallel because of the dipole fields arising from the magnetic poles at the edges of the bit. The intrinsic anisotropy, aligned at 45 degrees to the bit and word fields, determines the zero-field orientation. When a field is applied along the easy axis, as illustrated in (b), the moments at first remain unchanged, then spin-flop, and then scissor together to saturation. When a box-field excursion is applied, as in (c), the moments adiabatically rotate perpendicularly to the applied field, thus toggling the state of the bit.

at large fields because of the large exchange-coupling fields present in antiferromagnets. In the synthetic antiferromagnet configuration considered here, the coupling field, composed of the sum of the dipole and spacer exchange coupling, is substantially smaller, so that the spin-flop switching can be achieved at fields less than 100 Oe.

Figure 2(c) shows the operation of a toggle bit in an MRAM in the case of a "box-field" excursion. First the word-line field is turned on, which scissors the moments together, creating a net moment pointing roughly in the direction of the applied field. Hence, the axis along which the moments are anti-parallel rotates from the zero-field state by roughly 45 degrees. Then the bit-line field is turned on, which rotates each of the moments by roughly 45 degrees so that again the net moment is aligned with the applied field. Then the word-line field is removed, which continues the rotation of each moment another 45 degrees so that the net moment of the scissored moments is pointing along the bit-field direction. Finally the bit field is removed, and the moments relax into the AP state along the intrinsic anisotropy direction, but with their moments reversed from the starting condition. Hence, the state of the bit has been toggled, either from a "1" to a "0" or from a "0" to a "1." The toggle nature of this process requires that the MRAM circuit first read each bit before writing it to determine whether it has to be toggled. Compared to Stoner-Wohlfarth MRAM, this does increase the cycle time for the write operation; however, it also reduces the write power, since on average only half the bits have to be toggled.

### Simple perturbative model

We now describe a simple perturbative model which is useful for understanding the basic operation of toggle bits. The merit of this model lies in its simplicity—it is a one-dimensional model which is easy to visualize and interpret. The critical assumption made is that the dipole coupling field  $2M_sN$ , where  $M_s$  is the saturation magnetization and N is the demagnetization factor, is very large compared with the applied field H, which in turn is very large compared with the intrinsic anisotropy field  $H_i$ ; i.e.,  $2M_sN \gg H \gg H_i$ . Thus, the model is valid for thick layers with small  $H_i$  when fields around the spinflop point or smaller are applied. In particular, it does not describe the saturation of the moments at large fields. As an example, this model can be well applied to 200-nmdiameter, 6-nm-thick NiFe layers with  $H_i = 5$  Oe, where  $2M_sN = 474$  Oe. Errors in energy from this perturbative model compared with the exact single-domain model are then less than 10% for applied fields around 50 Oe or less; the spin-flop field  $H_{\rm sf}$  is calculated correctly to within 0.5% of the exact single-domain result. Additional assumptions are that the bit is circular and that both magnetic layers are of the same thickness t. All of these assumptions are lifted when we later consider the general case. However, throughout this paper, each magnetic layer is always assumed to be a single domain. This not only allows the use of a single degree of freedom for each layer to describe the energy, but also allows the use of simple demagnetization factors in the energy expression. The single-domain assumption is valid for very small magnetic layers, and a good approximation for the several-hundred-nanometer-sized devices of technological



Coordinate system for perturbative model. The intrinsic anisotropy (easy axis) is along the x-axis. The angles of the moments are denoted by  $\theta$  and  $\varepsilon$ , and that of the applied field by  $\alpha$ .

interest [8]. The single-domain behavior certainly breaks down as the thickness approaches some fraction of the width; however, for thin-film samples (perhaps 6 nm in thickness and 100–300 nm in width) the single-domain assumption is a good starting approximation.

**Figure 3** shows the coordinate system, with the easy axis ( $H_i$ ) along the x-direction. Thus, the bit fields and word fields are at 45 degrees to the x-direction. The applied field H is directed at an angle  $\alpha$  to the easy axis. The angle of the first moment is termed  $\theta$ , and the angle of the second is tracked by recording the angle  $\varepsilon$ , which is the amount by which the two moments deviate from being anti-parallel. The single-domain energy E is then

$$\begin{split} \frac{E}{M_{\rm s}At} &= -H[\cos{(\theta-\alpha)} - \cos{(\theta+\varepsilon-\alpha)}] \\ &- \left(M_{\rm s}N - \frac{J}{M_{\rm s}t}\right)\cos{\varepsilon} \\ &- \frac{1}{2}H_{\rm i}\cos^2{(\theta)} - \frac{1}{2}H_{\rm i}\cos^2{(\theta+\varepsilon)}, \end{split} \tag{1}$$

where A is the bit area, t is the thickness of the single layer, and J is the spacer layer exchange coupling. The first term is the Zeeman energy, arising from the interaction of the applied field with each of the moments. This term favors the alignment of each moment with the applied field. The second term is the coupling field energy, which is composed of two parts: the dipole coupling and the exchange coupling. This term favors an anti-parallel alignment of the two layers. Since these two coupling terms enter in the same way, we drop J in what follows, without loss of generality. The last two terms are the intrinsic anisotropy energy from each of the two layers. These two terms favor the alignment of each layer with the easy axis (x-axis).

We now make use of our assumption:  $2M_sN \gg H \gg H_i$ . We temporarily consider the case of no intrinsic anisotropy. Then, for a field applied along  $\alpha=0$ , the problem is easy to solve:  $H_x=2M_{\rm s}N\sin{(\epsilon/2)}\approx M_{\rm s}N\epsilon$ . For a field applied along an arbitrary direction, this generalizes to

$$\varepsilon = H\sin(\theta - \alpha)/(M_{s}N). \tag{2}$$

Alternatively (and more rigorously), one can expand Equation (1) in powers of  $H_i/M_sN$  and  $H/M_sN$ , retain only the leading terms, and minimize, thus obtaining Equation (2), correct to leading order. Using this expression for  $\varepsilon$  in Equation (1) leaves E as a function of only one variable,  $\theta$ . To leading order this gives

$$\frac{E}{M_{s}At} = -\frac{H^{2}}{2M_{s}N}\sin^{2}(\theta - \alpha) - H_{i}\cos^{2}\theta. \tag{3}$$

These two terms have very intuitive meanings. The first favors alignment of the moments perpendicular to the applied field, and the second favors alignment of the moments along the intrinsic anisotropy axis. Note also that the applied field appears only in second order. This is because to first order there is no net moment, and so there is no response to the applied field. However, to second order, the applied field itself creates a moment, and then this moment responds to the applied field. Finally, note that there is only one field scale in the problem, making it easy to guess the order of magnitude of the spin-flop field. From dimensional analysis, the spin-flop field must be of order  $(2H_iM_sN)^{1/2}$ , i.e., the geometric mean of the coupling field and the intrinsic anisotropy field. Again, this can be interpreted in terms of a net moment being created by the applied field (opposing the coupling field  $2M_sN$ ), and then rotating that moment (opposing the intrinsic anisotropy field  $H_i$ ).

Further substitution leads to the following even simpler expression for the energy, now in dimensionless units:

$$e = \frac{1}{2} [h^4 - 2h^2 \cos(2\alpha) + 1]^{1/2} \cos(2\theta - \varphi), \qquad (4)$$

where e is the dimensionless energy,  $e = E/(H_1M_sAt)$ , h is the dimensionless field,  $h = H/(2H_1M_sN)^{1/2}$ , and the phase  $\varphi$  is given by  $\tan \varphi = h^2 \sin 2\alpha/[h^2 \cos (2\alpha) - 1]$ . Hence, in this simple model, the energy landscape is always a simple sinusoid. The equilibrium value of  $\theta$  is given by the value at which Equation (4) is a minimum; i.e.,  $\theta = \varphi/2 + \pi/2$ . At that value of  $\theta$ ,  $\tan \varphi = \tan 2\theta$ ; thus,

$$\tan 2\theta = \frac{h^2 \sin 2\alpha}{h^2 \cos (2\alpha) - 1} \,. \tag{5}$$

Thus, there is only one discontinuity in  $\theta$  as a function of h, when the denominator of Equation (5) and the amplitude of Equation (4) vanish, at  $\alpha = 0$  and h = 1, as described in more detail later. The presence of a single discontinuity is in distinct contrast to what applies in

Stoner-Wohlfarth switching, where the moment switches at each point along the astroid curve because the energy minimum that the system is in ceases to be a minimum, and the system jumps discontinuously into another nearby minimum. This is shown schematically in Figure 4(a). The severe reduction in activation energy seen in Stoner–Wohlfarth switching, as shown in Figure 1(c), is a characteristic of this discontinuous type of switching; the system switches when the activation energy is reduced to zero. Figure 4(b) shows plots of Equation (4) for a number of different applied field values. The equilibrium value of  $\theta$  is given by the minimum in each curve, as traced out by the thick brown line. The energy curves are color-coded to correspond to the inset, which shows the field path. At zero field, the energy curve is shown in black. As the field is applied along the word axis, the system rotates to negative values of  $\theta$  (red curves). With each successive portion of the field path, the energy curve continues to translate to the left, corresponding to the clockwise rotation of the moments. The system is smoothly carried through the green curves, and then relaxes into the zero-field state as the field is reduced along the bit axis (for clarity, the corresponding energy curves are not shown). Hence, the moments have rotated by 180 degrees and have reversed state. As the field is applied, the moments rotate adiabatically in order to maintain themselves roughly perpendicular to the field.

The activation energy at all field values is given directly by twice the amplitude of Equation (4):

$$e_a = [h^4 - 2h^2 \cos(2\alpha) + 1]^{1/2},$$
 (6)

i.e., by the vertical distance between the minimum and maximum of each curve in Figure 4(b). From Figure 4(b) it is clear that the activation energy increases during half select (along the red series of curves). Furthermore, note that during the entire switching event the activation energy is maintained at a value larger than the zero-field value. Again, this is in distinct contrast to the Stoner–Wohlfarth case, where the activation energy vanishes at the switching field. The continuous nature of the switching event shown in Figure 4(b), as opposed to the discontinuous event shown in Figure 4(a), constitutes a major difference between toggle and Stoner–Wohlfarth switching.

**Figure 5** shows the one place where there is a discontinuity in switching: when Equation (6) equals zero; this occurs only when the field is applied along the easy axis ( $\alpha=0$ ), at a critical value  $h=h_{\rm sf}=1$ . Figure 5 shows energy curves for different values of the easy-axis field. At h=1, the minimum switches discontinuously from being at  $\theta=0$  to  $\theta=\pm\pi/2$  (i.e., the scissor state). The family of curves in Figure 5 explains the spin-flop behavior shown in Figure 2(b). For h<1, the energy minimum is at  $\theta=0$ .

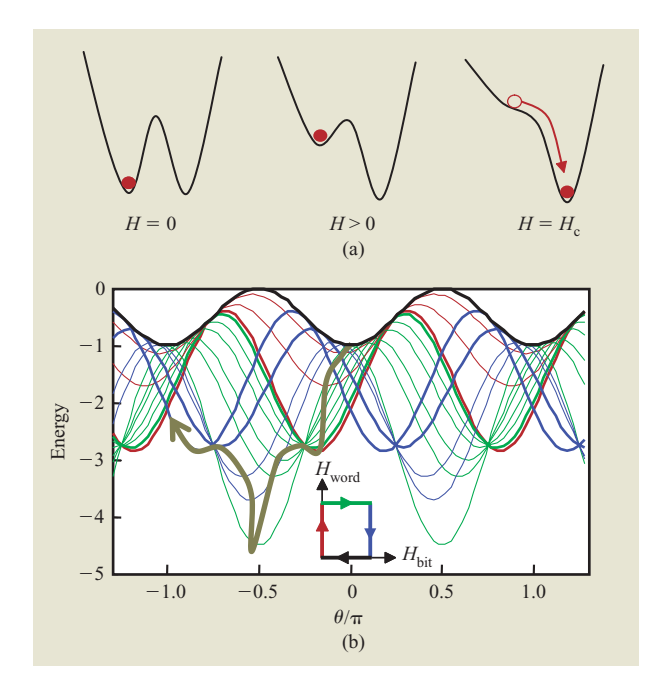
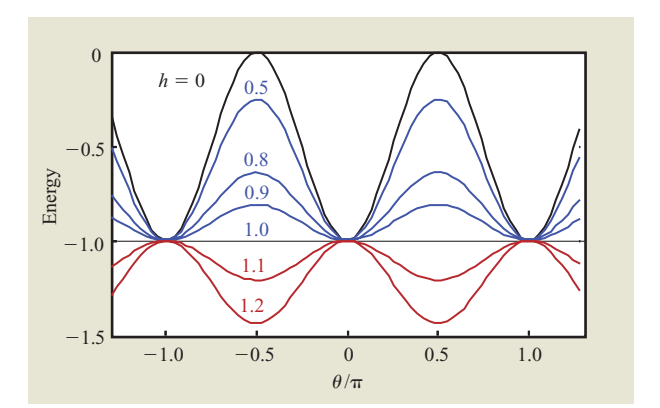


#### Figure 4

Energetics of Stoner–Wohlfarth switching vs. toggle switching. Stoner–Wohlfarth switching occurs discontinuously when the applied field changes the energy minimum into an inflection point (a). A toggle bit toggles without any discontinuities in the angle as a function of applied field (b). Curves of the dimensionless energy obtained from the perturbative model are color-coded, as indicated in the inset: black: zero-field energy; red: an increase in the word-line field only; green: the increase in the bit-line field; blue: the decrease in the word-line field. For clarity, the final set of curves, corresponding to the bit-line field being decreased, is not shown.

At h = 1, the system abruptly jumps into the scissored state at either  $\theta = \pi/2$  or  $\theta = -\pi/2$ . Furthermore, Figure 5 can be used to understand the general criterion for toggling. Toggling requires passing through the state  $\theta = \pi/2$  (or  $-\pi/2$ ). From Equation (5), this can happen only when  $\alpha = 0$ ; i.e., the field is applied along the easy axis. When the field is along the easy axis (see Figure 5), the state at  $\theta = \pi/2$  is a minimum only if h > 1. Hence, the criterion for toggling is that the field excursion must cut across the easy axis at h > 1. This is shown as a red ray in Figure 6, drawn with the x- and y-axes as the bitline and word-line fields (so that the easy axis is along the 45-degree line). From the figure it is clear that the toggling criterion is equivalent to requiring the field excursion to enclose the spin-flop point, defined by  $\alpha = 0$ , h = 1, denoted by the red dot in Figure 6. Furthermore, if one is restricted to rectangular field excursions (changing  $h_x$  and  $h_y$  only separately), the toggling criterion defines an L-shaped critical curve shown in blue in Figure 6. For rectangular field excursions (starting at zero field) which





Energy curves, from the perturbative model, for the field applied along the easy axis; again, energy is dimensionless, and the zero-field case is shown in black. As the field is increased, the minimum continues to be at  $\theta=0$  (blue curves) until, for h>1, the minimum discontinuously jumps to  $\theta=\pi/2$  (red curves).

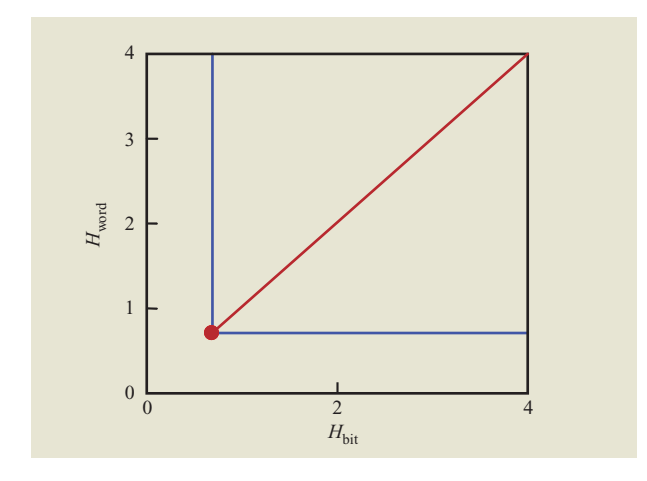


#### Figure 6

Combined effects on switching of word and bit fields. The red dot is the spin-flop point; this or the red ray extending from the spin-flop point defines the switching criterion for arbitrary field excursions (see text). The field values are normalized to  $(2H_{\rm i}M_{\rm s}N)^{1/2}$ . For rectangular field excursions, the red ray defines the blue L-shaped critical switching curve.

cross this critical switching curve, the system toggles, whereas for rectangular field excursions which do not cross this critical switching curve, the system does not toggle. Note that this model explicitly ignores the effects of large fields (i.e., what occurs at saturation) because of the assumption that  $2M_sN \gg H$ . Therefore, the manner in which the critical switching curve behaves at large fields

is outside this perturbative model and requires analysis using the exact single-domain theory, discussed next.

To summarize this section: The analyses indicate that there are no discontinuities in  $\theta$  as a function of applied field, except at the spin-flop point. Instead, the moments rotate adiabatically and perpendicularly to the applied field. The activation energy increases under half select, thus eliminating the activated-error problem, and the critical switching curve for rectangular field excursions has a perfect L shape, which reduces the half-select margin problem.

## **Exact single-domain model**

We now turn our attention to an exact solution of the single-domain two-layer problem, which has been discussed in [3] and [4]. The energy can be written, again in reduced units, as

$$\begin{split} e(\theta_{1},\theta_{2}) &= -h_{x}[z\cos\theta_{1} + \cos\theta_{2}] - h_{y}[z\sin\theta_{1} + \sin\theta_{2}] \\ &+ (n_{x} - jz)\cos\theta_{1}\cos\theta_{2} + (n_{y} - jz)\sin\theta_{1}\sin\theta_{2} \\ &+ \frac{z}{2}(n_{y} - n_{x} + h_{i})\sin^{2}\theta_{1} \\ &+ \frac{1}{2z}(n_{y} - n_{x} + h_{i}z)\sin^{2}\theta_{2} \,, \end{split} \tag{7}$$

where  $e = Eb/\pi^2 M_s^2 abt_1 t_2$ ,  $h_{x,y,i} = H_{x,y,i} b/4\pi M_s t_1$ ,  $j = Jb/4\pi M_s^2 t_1^2$ ,  $z = t_1/t_2 > 1$ , E is the energy,  $\theta_{1,2}$  are the angles of the moments of the two layers measured from the x-axis,  $H_i$  is the intrinsic anisotropy in the  $\hat{x}$ -direction,  $t_{1,2}$  are the thicknesses, a is the length in the  $\hat{x}$ -direction, b is the width in the  $\hat{y}$ -direction,  $n_{x,y}$  are the reduced demagnetizing factors in the  $\hat{x}$ - and  $\hat{y}$ -directions,  $M_s$  is magnetization, J is the exchange coupling between the layers, and  $H_{x,y}$  are the applied fields in the  $\hat{x}$ - and  $\hat{y}$ directions. Throughout this section, fields in lowercase are in reduced units; conversion to CGS units can be achieved by using  $H = h4\pi M_s t_1/b$ . The minima of Equation (7) define the equilibrium values of  $\theta_1$  and  $\theta_2$ . As the field is applied, these minima shift position, corresponding to the moments rotating, and sometimes change stability from being a minimum to being a saddle point, corresponding to discontinuous switching events. Given a critical point, it is possible to calculate the critical fields at which these stability changes occur by calculating the discriminant of Equation (7) and setting it to zero:

$$e_{\theta_1 \theta_1} e_{\theta_2 \theta_2} - (e_{\theta_1 \theta_2})^2 = 0.$$
 (8)

This condition corresponds to either a minimum or a maximum changing into a saddle point. For  $h_y=0$  (i.e., easy-axis field only), it is easy to show that the parallel (P) states  $(\theta_1, \theta_2) = (0, 0)$ ,  $(\pi, \pi)$  and the anti-parallel (AP) states  $(0, \pi)$ ,  $(\pi, 0)$  are always critical points of Equation (7) by showing that  $e_{\theta_1}=0$  and  $e_{\theta_2}=0$  at these values of  $(\theta_1, \theta_2)$ . Evaluating Equation (8) at these values

of  $(\theta_1, \theta_2)$  and solving for  $h_x$  gives the following switching fields: For positive fields, the AP states lose stability at

$$\begin{split} h_{\rm sf} \\ \text{or} \\ h_{\rm d} \\ \end{pmatrix} &= \left\{ h_{\rm i} \left[ (n_{\rm y} - jz) \left( 1 + \frac{1}{z} \right) + h_{\rm i} \right] \right. \\ &+ \left. \left( \frac{n_{\rm y} - jz}{2} \right)^2 \left( 1 - \frac{1}{z} \right)^2 \right\}^{1/2} \\ &\pm \frac{1}{2} \left( 1 - \frac{1}{z} \right) (2n_{\rm x} - n_{\rm y} - jz), \end{split} \tag{9}$$

where the  $\pm$  of the  $\pm$  sign refers to  $h_{\rm sf}$  and the - to  $h_{\rm d}$ . The spin-flop field  $h_{\rm sf}$  corresponds to the  $(0,\pi)$  state losing stability, and the direct-write field  $h_{\rm d}$  corresponds to the  $(\pi,0)$  state losing stability (since  $z=t_1/t_2>1$ ,  $h_{\rm d}$  corresponds to the thickness-imbalance unfavored state losing stability). For positive fields, the P state (0,0) loses stability at

$$h_{xsat} = (1 + 1/z)(n_x - jz) - h_i. {10}$$

Next we consider the simple case in which the two layers have the same thickness: z = 1. Then  $h_{\rm sf} = h_{\rm d}$ , and Equations (9) and (10) reduce to Equation (11) (now with units):

$$H_{\rm sf} = \left[ H_{\rm i} \left( 8\pi M_{\rm s} n_{y} \frac{t}{b} - \frac{2J}{M_{\rm s} t} + H_{\rm i} \right) \right]^{1/2}, \tag{11}$$

$$H_{xsat} = 8\pi M_{s} n_{x} \frac{t}{b} - \frac{2J}{M_{c}t} - H_{i}. \tag{12}$$

Similarly for z = 1, the field at which the moments saturate in the y-direction, i.e., at which the  $(\pi/2, \pi/2)$  state loses stability, is given by

$$H_{ysat} = 8\pi M_{s} n_{y} \frac{t}{b} - \frac{2J}{M_{s} t} + H_{i}.$$
 (13)

One can see that the spin-flop field is the geometric mean of the intrinsic anisotropy and the hard-axis saturation field. This is in agreement with the discussion in the perturbative calculation section above: regarding the applied field as first creating a net moment and then rotating against the intrinsic anisotropy. In particular, note that the spin-flop field involves the hard-axis saturation field and not the easy-axis saturation field; this makes sense because in zero field the moments lie along the x-axis, and to create a net moment they must be canted toward the y-axis, i.e., toward the hard-axis direction. The saturation fields also make intuitive sense; the applied field must overcome both the dipole coupling and the exchange coupling to make the moments become parallel. Furthermore, in the x-direction (easy axis), the intrinsic anisotropy assists the applied field, resulting in a minus sign for the  $H_i$  term, whereas in the y-direction

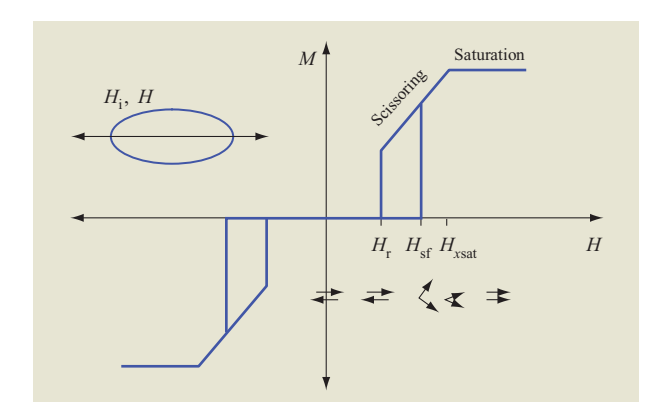


#### Figure 7

Easy-axis hysteresis loop at zero temperature calculated from the exact single-domain model for the case of a circle with  $t_1 = t_2$ . Inset shows the coordinate system: the intrinsic anisotropy, applied field, long axis of the ellipse, and x-axis are all parallel.

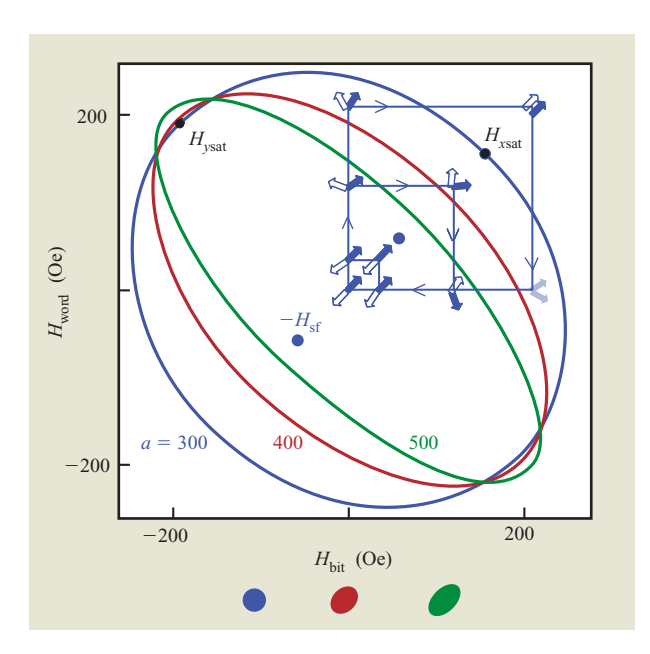
(hard axis) it opposes it, resulting in a plus sign for the  $H_i$  term.

**Figure 7** shows the corresponding easy-axis hysteresis loop for the case z=1. Note that there is some hysteresis as the field is decreased from saturation, because the moments return in the scissoring state, which continues to be a minimum down to a field  $H_r$ . For fields  $H_r < H < H_{sf}$ , there are therefore two (four with degeneracy) possible states: the AP state and the scissoring state. The system does not return to the AP state until the scissoring state ceases to be a minimum, at the return field  $H_r$ . This field can be calculated as follows: 1) by noting that on the easy axis, for the scissoring state,  $\theta_1 = -\theta_2$ ; and 2) by minimizing Equation (7) subject to this constraint. Equation (8) can then be evaluated at the resulting critical point and solved for  $H_x = H_r$ . This procedure gives

$$H_{\rm r} = \left(8\pi M_{\rm s} n_{\rm x} \frac{t}{b} - \frac{2J}{M_{\rm s} t} - H_{\rm i}\right)$$

$$\times \left(\frac{H_{\rm i}}{8\pi M_{\rm s} n_{\rm y} \frac{t}{b} - \frac{2J}{M_{\rm s} t} + H_{\rm i}}\right)^{1/2}.\tag{14}$$

From Equation (14) it is clear that the amount of hysteresis decreases with decreasing aspect ratio and is very small for circles, where  $n_x = n_y$  (note that for technologically relevant samples,  $H_i$  is much smaller than the dipole coupling fields). Note that in practice it is  $H_{\rm sf}$  and not  $H_{\rm r}$  that determines the toggling criterion, since for field excursions between  $H_{\rm r}$  and  $H_{\rm sf}$  the moments can stay in the AP state and hence not toggle. See [5] for a



Saturation boundary as a function of aspect ratio for the case  $t_1 = t_2$ , calculated using the exact single-domain model with  $t_1 = t_2 = 2.5$  nm,  $M_{\rm s} = 1,500$  emu/cc, b = 300 nm,  $H_{\rm i} = 25$  Oe, and J = 0. The three shapes of length a, shown at the bottom of the figure, correspond to a = 300,400, and 500 nm. Larger aspect ratios result in a more elliptical saturation boundary. For the circle, the spin-flop points and  $H_{\rm ssat}$  and  $H_{\rm ysat}$  are also shown. Three rectangular field excursions are also shown for the circle, demonstrating the three types of behavior as a function of excursion size. Adapted from [4], with permission; ©2004 American Institute of Physics.

more detailed discussion. Also note that Figure 7 is drawn for zero temperature. Since the activation energy goes to zero at the spin-flop point, the measured hysteresis loop depends on the speed of the field sweep, as is the case for Stoner–Wohlfarth switching. Slower field sweeps result in a smaller measured  $H_{\rm sf}$ .

**Figure 8** shows the saturation boundary, defined as the field at which the two moments become parallel, for an arbitrary field direction. In the easy-axis and hard-axis directions, the saturation field is given by  $H_{xsat}$  and  $H_{ysat}$ . Figure 8 was calculated numerically as described in [4], but for technologically relevant samples, the saturation curve is an ellipse, to within less than one percent. Since the moments are parallel for fields larger than the saturation boundary, for a balanced bit (z=1), any data stored in the bit is lost. For the blue curve, Figure 8 shows three examples of rectangular field excursions. For field excursions small enough not to contain the spin-flop point, the bit is not toggled. For intermediate-sized field excursions which do contain the spin-flop point but which do not cross the saturation boundary, the bit is toggled.

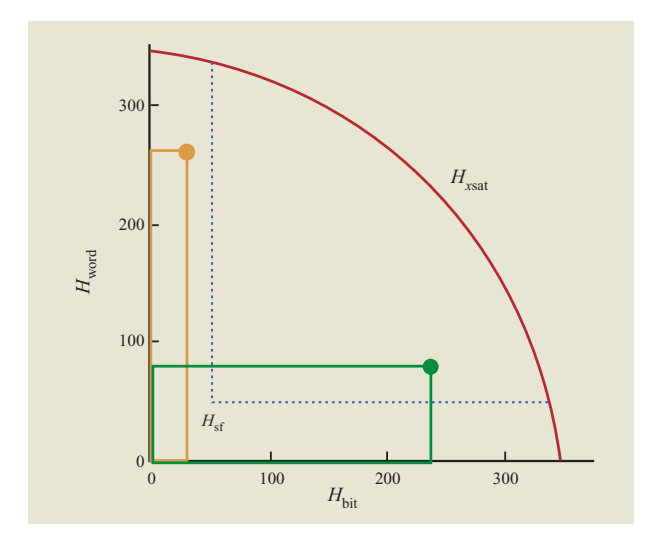


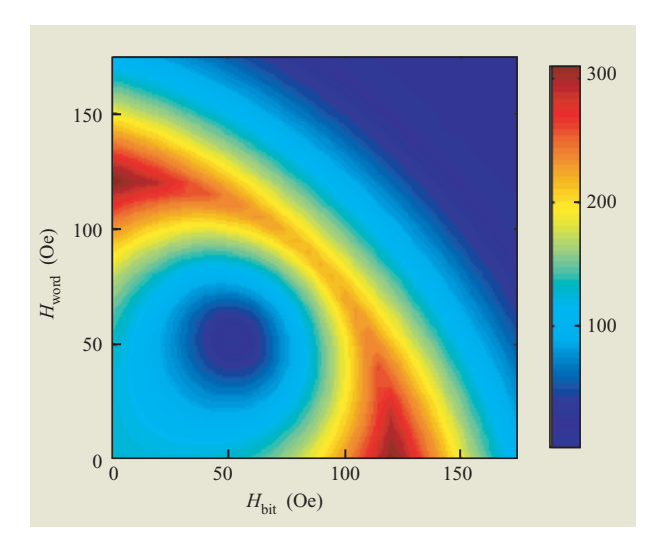
#### Figure 9

Critical switching curve calculated using the exact single-domain model for the case of a circle with  $t_1 = t_2$ . In addition to the low-field behavior predicted by the perturbative model (see Figure 6), this figure also shows the saturation boundary. For rectangular field excursions, the switching boundary has an ideal L shape, terminated at the saturation boundary.

Finally, for large field excursions which do cross the saturation boundary, the data is lost—the bit returns to one of the two AP states, but for a perfectly balanced sample, the result is random. Note that the bits can be toggled by field excursions in either the first or the third quadrant, and that both quadrants do not have to be used to write into both the "0" and "1" states. This is another advantage of toggle MRAM over Stoner—Wohlfarth MRAM: Only unidirectional current drivers are required for toggle MRAM.

**Figure 9** shows the resultant critical switching curve for a balanced bit with rectangular field excursions. The field plane is naturally divided into three regions. For fields smaller than the blue-dotted L-shaped curve (e.g., the orange field point), nothing occurs. For fields larger than the blue-dotted L-shaped curve but smaller than the red saturation boundary (e.g., the green field point), the bit toggles. For fields larger than the red saturation boundary, the data is scrambled.

Equation (7) can also be used to calculate the activation energy. As discussed in [4], this can be done analytically for fields along the easy axis and numerically at arbitrary fields. The results are shown in **Figure 10**, as a function of the bit-line and word-line fields, for a circular bit with  $t_1 = t_2$ . **Figure 11(a)** shows two cuts across Figure 10, one along the easy axis and the other along the bit-line or word-line direction. When activating over the AP saddle point of the figure at low fields, the moments



Activation energy (kT) as a function of bit and word fields. Calculated for a circular bit 300 nm in diameter, with  $t_1=t_2=2.5$  nm,  $M_{\rm S}=1,500$  emu/cc,  $H_{\rm i}=25$  Oe, and J=0. Adapted from [4], with permission. ©2004 American Institute of Physics.

maintain their roughly anti-parallel orientation during activation, whereas when activating over the P saddle point at larger fields, the moments pass through the parallel state. From these figures it is clear that the activation energy initially increases under half select (when the field is applied along the bit-line or word-line direction). The activation energy goes to zero at the spinflop point and also at large fields along the saturation boundary. One can distinguish two distinct regions in the activation energy as a function of applied field; see for example the half-select curve shown in Figure 11(a). For small fields, the moments activate through the AP saddle point, as shown in Figure 11(b). At these small fields the moments are not significantly canted together, and so they activate by staying substantially anti-parallel and rotating together into the opposite state. At larger fields, however, the moments are significantly canted together, and so they activate by exchanging positions, i.e., by passing through the P saddle point. Note that the increase in activation energy under half select shown in Figure 11(a) is one of the key features which distinguishes toggle MRAM from Stoner-Wohlfarth MRAM.

Equation (9) can be used to calculate the spin-flop and direct-write fields for the case in which  $z \neq 1$ . In this case, for fields along the easy axis, the bit switches from one AP state to the other at a field  $H_{\rm d}$ , spin-flops at a larger field  $H_{\rm sf}$ , and then saturates at an even larger field  $H_{\rm xsat}$ , as discussed in [4]. This is shown in **Figure 12** for the case of a circular bit. The field scale is  $\pm 230$  Oe. The loop was calculated assuming that  $t_1 = 2.5$  nm,  $t_2 = 2$  nm,

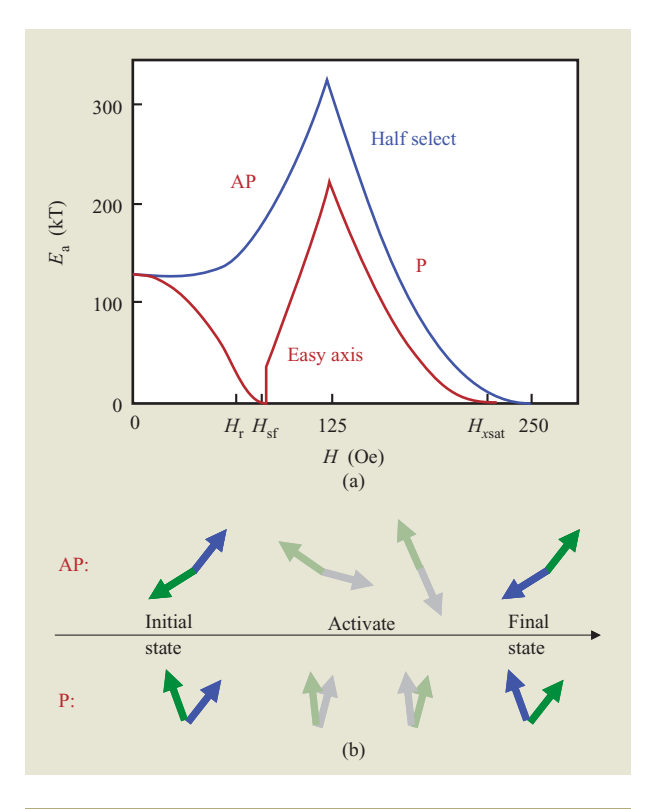
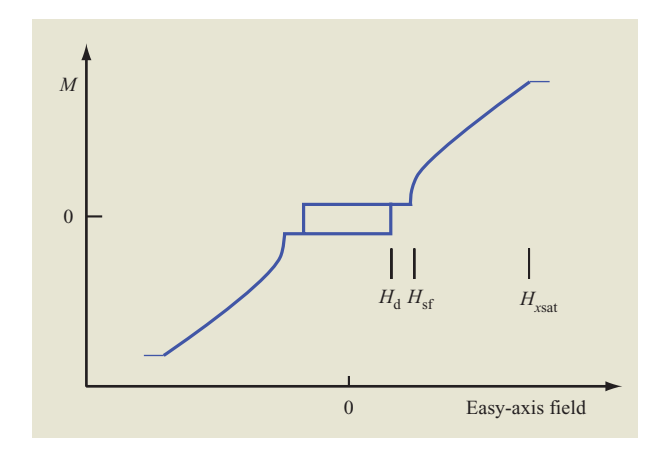


#### Figure 11

(a) Activation energy cuts along the easy-axis and half-select directions, from Figure 10. There are two different saddle points, resulting in the two different activation energy regions as a function of applied field, labeled AP and P. (b) The associated activation paths. Adapted from [4], with permission; ©2004 American Institute of Physics.

 $M_s = 1,500 \text{ emu/cc}, a = b = 300 \text{ nm}, H_i = 15 \text{ Oe}, \text{ and } J = 0.$ 

Note that at small fields both AP states are stable, but for larger fields only one state is stable (the state with the thicker moment pointing in the applied field direction). Furthermore, if one considers arbitrary fields, there is a region in field space inside which only one magnetic state exists, as shown in Figure 13 by the heart-shaped regions outlined in black. This direct-write state has the thicker moment pointing roughly in the direction of the applied field and the thinner moment roughly anti-parallel. Outside this direct-write region there always exist at least two magnetic states; for example, along the easy axis near zero field there are the two AP states  $(0, \pi)$  and  $(\pi, 0)$ . The consequence is that when a field excursion crosses the direct-write boundary, the bit always ends up in the direct-write state and, upon returning to zero field, reaches the thickness-favored state  $(0, \pi)$  for fields applied in the first quadrant. Thus, this direct-write region must be avoided when toggling. Figure 13 shows the resulting



Easy-axis hysteresis loop, for a circular bit, calculated from the exact single-domain model, for the case  $t_1 > t_2$ .

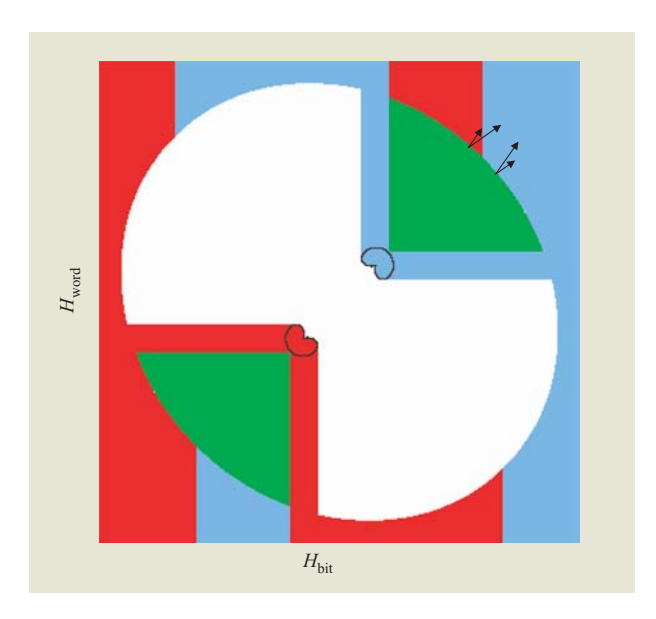


## Figure 13

Critical switching curve for rectangular field excursions calculated using the exact single-domain model for the case of a circle and  $t_1 > t_2$ .

critical switching curves for rectangular field excursions. The bit toggles in the green regions, does not change in the white region, direct- or saturation-writes into the  $(0, \pi)$  state in the blue regions, and direct- or saturation-writes into the  $(\pi, 0)$  state in the red regions. The field scales are  $\pm 400$  Oe. The curves were calculated assuming that  $t_1 = 4.1$  nm,  $t_2 = 3.5$  nm,  $M_{\rm s} = 1,500$  emu/cc, a = b = 300 nm,  $H_{\rm i} = 25$  Oe, and J = 0.

Again, for small field excursions nothing occurs. For intermediate-sized field excursions, the direct-write region defines an L-shaped direct-write area. Any field excursion inside this direct-write area results in a direct write to the thickness-favored state  $(0, \pi)$ . At fields large enough to completely circumnavigate the direct-write region, the bit toggles. At still larger fields, which cross the saturation boundary, the bit saturation writes. This means that, regardless of the initial state, upon crossing the saturation boundary the bit reaches the thickness-favored state, which determines the state returned to in zero field. Hence, this should be avoided in a toggle MRAM. For the most part, the bit saturation writes into the thicknessfavored state of  $(0, \pi)$  for the first quadrant and the adjoining regions of the second and fourth quadrants, and  $(\pi, 0)$  elsewhere. There is a small region in the first quadrant that saturation-writes to the  $(\pi, 0)$  state because of the thicker moment points on the intrinsic anisotropy side of the applied field as the field returns through the saturation boundary and the thinner moment points on the other side of the applied field. This is shown in Figure 13 for two examples on either side of the intrinsic anisotropy direction. During the rest of the field excursion, the moments continue to rotate through the toggle region and thus reach the  $(0, \pi)$  state if they cut across the saturation boundary at a bit field  $H_{\rm bit} > H_{\rm xsat}/\sqrt{2}$  or the  $(\pi, 0)$  state if they cut across the saturation boundary at a bit field  $H_{\text{bit}} < H_{x\text{sat}}/\sqrt{2}$ . Note, however, that for bit fields small enough not to cut through the direct-write region, the saturation write is again into the thickness-favored state because the bit relaxes into the AP state and not the scissoring state. Note that in Figure 13 the horizontal and vertical lines are an artifact of the restriction to rectangular field excursions that turn on the word-line field first, then turn on the bit-line field, then turn off the word-line field, and then turn off the bitline field. The fundamental physical quantities are the direct-write region, saturation boundary, and intrinsic anisotropy direction. If these are known, the critical switching curves can be calculated for arbitrarily shaped field excursions.

#### Summary

We have presented an overview of the use of a single-domain model in understanding the switching behavior for spin-flop bits, including the spin-flop and direct-write fields, saturation boundary, and direct-write region, thus enabling us to predict the resulting critical switching curves. In particular, the model predicts that for rectangular field excursions (changing only  $H_x$  or  $H_y$ , one at a time), toggle bits have an ideal L-shaped critical switching curve, which allows fields along the bit or word field direction to be several times larger than the full-select field without disturbing the bit. In addition, the

model shows that the activation energy increases under half select, which should eliminate the half-select activated-error problem. Also, the almost zero net moment of the free layers minimizes cell-to-cell magnetostatic coupling. These factors should make toggle bits attractive for multi-megabit MRAMs.

### **Acknowledgments**

The author would like to thank David Abraham for help in understanding the saturation switching behavior shown in Figure 13. Portions of this work were completed as part of the IBM/Infineon MRAM Development Alliance.

#### References

- 1. S. S. P. Parkin, K. P. Roche, M. G. Samant, P. M. Rice, R. B. Beyers, R. E. Scheuerlein, E. J. O'Sullivan, S. L. Brown, J. Bucchignano, D. W. Abraham, Yu Lu, M. Rooks, P. L. Trouilloud, R. A. Wanner, and W. J. Gallagher, J. Appl. Phys. 85, 5828 (1999); M. Durlam, P. Naji, A. Omair, M. DeHerrera, J. Calder, J. M. Slaughter, B. Engel, N. Rizzo, G. Grynkewich, B. Butcher, C. Tracy, K. Smith, K. Kyler, J. Ren, J. Molla, B. Feil, R. Williams, and S. Tehrani, Digest of Technical Papers, IEEE Symposium on VLSI Circuits, 2002, p. 158; A. R. Sitaram, D. W. Abraham, C. Alof, D. Braun, S. Brown, G. Costrini, F. Findeis, M. Gaidis, E. Galligan, W. Glashauser, A. Gupta, H. Hoenigschmid, J. Hummel, S. Kanakasabapathy, I. Kasko, W. Kim, U. Klostermann, G. Y. Lee, R. Leuschner, K.-S. Low, Y. Lu, J. Nutzel, E. O'Sullivan, C. Park, W. Raberg, R. Robertazzi, C. Sarma, J. Schmid, P. L. Trouilloud, D. C. Worledge, G. Wright, W. J. Gallagher, and G. Muller, Digest of Technical Papers, IEEE Symposium on VLSI Technology, 2003, p. 15.
- 2. M. Durlam, D. Addie, J. Akerman, B. Butcher, P. Brown, J. Chan, M. DeHerrera, B. N. Engel, B. Feii, G. Grynkewich, J. Janesky, M. Johnson, K. Kyler, J. Motia, J. Marti, K. Nagel, J. Ren, N. D. Rizzo, T. Rodriguez, L. Savtchenko, J. Salter, J. M. Slaughter, K. Smith, J. J. Sun, M. Lien, K. Papworth, P. Shah, W. Qin, R. Williams, L. Wise, and S. Tehrani, Digest of Technical Papers, IEEE International Electron Devices Meeting, 2003, p. 995.

- D. C. Worledge, Appl. Phys. Lett. 84, 2847 (2004).
  D. C. Worledge, Appl. Phys. Lett. 84, 4559 (2004).
  H. Fujiwara, S.-Y. Wang, and M. Sun, Trans. Magn. Soc. Jpn. 4, 121 (2004).
- 6. B. N. Engel, J. Akerman, B. Butcher, R. W. Dave, M. DeHerrera, M. Durlam, G. Grynkewich, J. Janesky, S. V. Pietambaram, N. D. Rizzo, J. M. Slaughter, K. Smith, J. J. Sun, and S. Tehrani, IEEE Trans. Magn. 41, 132 (2005).
- 7. M. Motoyoshi, I. Yamamura, W. Ohtsuka, M. Shouji, H. Yamagashi, M. Nakamura, H. Yamada, K. Tai, T. Kikutani, T. Sagara, K. Moriyama, H. Mori, C. Fukamoto, M. Watanabe, R. Hachino, H. Kano, K. Bessho, H. Narisawa, M. Hosomi, and N. Okazaki, Digest of Technical Papers, IEEE Symposium on VLSI Technology, 2004, p. 22.
- 8. R. P. Cowburn, J. Magn. Magn. Mater. 242-245, 505 (2002).

Received February 25, 2005; accepted for publication May 13, 2005; Internet publication January 6, 2006

**Daniel C. Worledge** *IBM Research Division, Thomas J.* Watson Research Center, P.O. Box 218, Yorktown Heights, New York 10598 (worledge@us.ibm.com). Dr. Worledge received a B.A. degree with a double major in physics and applied mathematics from the University of California at Berkeley in 1995. He received a Ph.D. degree in applied physics from Stanford University in 2000, with a thesis on spin-polarized tunneling in oxide ferromagnets. After joining the Physical Sciences Department at the IBM Thomas J. Watson Research Center as a postdoctoral researcher, he became a Research Staff Member in 2001, working on fast-turnaround measurement methods for magnetic tunnel junctions. In 2003, Dr. Worledge became the manager of the MRAM Materials and Devices group. His current research interests include magnetic devices and their behavior at small dimensions.